A HYDRAULIC MODEL OF A LIVESTOCK WASTE FLUSHING SYSTEM

Thesis for the Degree of M. S.

MICHIGAN STATE UNIVERSITY

RONALD JAMES BALLARD

1977

ABSTRACT

A HYDRAULIC MODEL OF A LIVESTOCK
WASTE FLUSHING SYSTEM

By

Ronald James Ballard

A hydraulic model of the waste flushing system at the Michigan State University Swine Research Center was constructed and analyzed. The object was to simulate feces transport under the varying input parameters of dump volume, dump tank height, and distance from the tank to the back wall. Mathematical analysis and computer simulation were investigated and deemed inappropriate for this study. The model was constructed of plexiglass.

Verification of the model consisted of two phases: fixed-bed verification, and movable-bed verification. Fixed-bed verification involved filming the hydraulic flow in both the prototype and the model with no sediment load. The model was adjusted to mimic the prototype by reducing the dump volume and adding surface roughness. Verification of the model in the movable-bed state was accomplished by determining the particle diameter scale ratio for correct sediment transport

characteristics in the model. A modification of the Froude number is proposed as a possible theoretical explanation of the particle diameter scale ratio.

The model, being verified for sediment flow, is now ready to be used for data collection to determine the trade-offs in input parameters.

Approved John B. Herreid
Major Professor

Approved D. R. Haldeman
Department Chairman

A HYDRAULIC MODEL OF A LIVESTOCK WASTE FLUSHING SYSTEM

By

Ronald James Ballard

A THESIS

Submitted to
Michigan State University
in partial fulfillment of the requirements
for the degree of

MASTER OF SCIENCE

Department of Agricultural Engineering

1977

ACKNOWLEDGMENTS

I would like to thank several people who gave me immeasurable assistance during my graduate work at Michigan State:

Chuck Shubert, Jim Steffe, and Dale Thompson who were fellow C.R.A.P. crew members and offered many ideas and a lot of support.

Shari Cisco, Howard Doss, Dave Hamilton, Kathy Kacynski, Don Miles, Joe Panci, John Panci, Jean Purnell, Sue Steffe, and Julie VanderHaagen, who as friends offered their support and encouragement during times of crisis.

Ted Loudon and David McIntosh for serving on my committee and offering me professional advice and direction.

Dennis Heldman for being a truly understanding Department Chairman.

Doug Coulter and Joyce Metsa for doing some rather unpopular work with me.

The biggest thank-you goes to John Gerrish, who as my major professor was all of the above and more--a model human being.

TABLE OF CONTENTS

LIST OF TABLES

LIST OF FIGURES

LIST OF SYMBOLS

A	Maximum cross-sectional area of flow
d	Particle diameter
D	Depth of flow
H	Height from floor to dump tank pivot point
n	Manning's roughness factor
P	Wetted perimeter
Q	Discharge
R	Hydraulic radius
S	Slope
S_s	Specific weight of sediment
T	Time
v	Velocity
W	Width of flow
X	Horizontal [length (L), width (W)]
Y	Vertical [height (H), depth (D)]
α	Effective weight of sediment (S_s - 1)
τ	Shear at bed caused by flow over particles
ν	Kinematic viscosity
m	Model variable (subscript)
p	Prototype variable (subscript)
r	Ratio of parameters (prototype/model) (subscript)

' Parameter associated with intrinsic roughness (superscript)

" Parameter associated with form (e.g., dune) roughness (superscript)

Units

1 centistoke (cs) = 1×10^{-6} m^2/s (ν - kinematic viscosity)

1 foot (ft) = 0.3048 meter (m)

1 inch = 2.540 centimeters (cm)

1 gram/cubic centimeter = 62.4 pounds/cubic foot

I. INTRODUCTION

Hydraulic transport of livestock feces is being adopted nationally as well as in Michigan (Carlisle, 1976). Advantages of hydraulic waste transport (termed "flushing") include odor control within the building, reduction of manual labor, and a direct tie-in to an anaerobic lagoon.

There are two basic ways for livestock producers to use flushing as a manure transport system: open-alley (or gutter) flushing and under-slat flushing. Open-alley flushing is primarily used by dairy farmers in free-stall barns and open-gutter flushing is usually used by pork producers (Jones et al., 1971). Under-slat flushing is used by some Michigan pork producers. In this system, hogs are grown on slats and the manure drops through slots between the slats to a sloping alley below. One of the advantages of this system is separation of hogs from the flushing water avoiding possible transmittance of disease.

There are several ways to release the water used for flushing. Some of the more common methods are releasing elevated water through a large siphon pipe, opening a quick-release door on a non-elevated tank, and using a non-symmetrical tank on a horizontal pivoting axis that tips and self-dumps when full. If elevated, the tank tips into a curve that directs it down the alley. The sytem analyzed herein, described by Miller and Hansen (1974), is an under-slat flushing system that utilizes an elevated tipping tank for water release.

This study was prompted by the rising popularity of this waste-handling method and the need for design criteria based upon engineering analysis. The lack of design information has contributed to the operational inefficiency on some Michigan farms. The parameters considered important are flush length (L), height of the tip-tank (H), water volume released (Q), and the distance from the tank to the curved wall against which it dumps. My purpose in this study is to develop a model that will simulate the actual system at the Michigan State University Swine Research Center (termed the "prototype") with respect to the above variable parameters. I investigated mathematical analysis, computer simulation, and physical (scale) modeling as methods of system interpretation and engineering analysis.

II. LITERATURE REVIEW

Flushing Literature

Literature containing design criteria for flushing systems has, to date, been sparse; the design criteria are largely empirical. George and Browning (1973) presented tables for flushing units similar to the one studied here. They propose a flow depth of five to ten centimeters for a ten-second duration. This requires variable width and variable slope open gutters, and includes hydraulic resistance caused by manure and by pigs standing or lying in the gutters. Their results are not readily applicable to under-slat flushing. Jones (1971) studied hydraulic waste transport in a channel fed by a siphon discharge; their goal was to establish a minimum flushing volume. Their studies suggest the advantage of higher-velocity flows in conserving water. Their data collection technique included the use of movie film exposed in an actual flushed barn; a similar technique is used in this study.

A very important point can be drawn from the paper by Jones et al. (1971); the volume of water used in each flush can be reduced if the water velocity down the alley is increased. Water moving at higher velocities has greater sediment transport capacity. Somewhat greater water velocities may be obtained in two ways: (1) dumping from a higher location to give the water a higher potential energy; and (2) faster release of the water to give a greater flow depth, which helps maintain higher velocities. The tipping tank releases water much faster than a siphon or drop-gate apparatus and elevating the tank increases the potential energy of the water. Thus, the elevated tipping tank would seem to make most efficient use of the water to be released.

Modeling Literature

There is little literature available dealing with the mathematical description of a sudden surge wave flowing down a dry slope. Chow (1959) treats rapidly varying, unsteady flow. Henderson (1966) outlines a dam-break problem under the idealized conditions of unlimited reservoir and friction-free flow. However, in my case, friction is a major factor in determining flow characteristics and the water released by the tip tank is far from unlimited. The differential equations for unsteady open-channel flow which might apply to this study can be found in Streeter and Wiley (1967) but the equations lead to a mathematically intractable result. Computer simulation of the resulting differential equations would be time consuming (due to the limited volume reservoir) and therefore expensive. Both mathematical analysis and computer simulation are further complicated to a great degree when the cohesive sediment is added. Both methods of analysis would have to deal with three regimes of flow: (1) threshold of movement, (2) suspended load (particles in motion), and (3) stable channel (all particles to be moved are moved). Due to the extreme difficulties associated with mathematical analysis and computer simulation in this study, a scaled-down physical model is a more appropriate analytical tool.

Model Scaling Analysis

There are two types of physical model treated in the literature: fixed-bed and movable-bed. A fixed-bed model is one used for modeling structures where there is no movement other than the water; all model boundaries are stable. Examples would be dams and spillways. Movable-bed modeling involves the analysis of systems with non-stable boundaries; sediment transport requires a movable-bed approach. The usual application is in modeling river and harbor systems. Fixed-bed analysis is considerably simpler and there is more literature available.

A problem in surge or wave models is that both Froude and Reynolds numbers must be held constant during scale-up or scale-down. Doherty and Franzini (1965) state that the Reynolds number (Re) must be high enough to maintain turbulence in the model where there is such turbulence in the prototype. In the flushing system, however, shallow flow in the prototype limits turbulence to the wave front. Keeping this turbulence in the model may be a problem. For this reason, a distorted model (i.e., a model in which the vertical and horizontal scale factors are unequal) is appropriate.

Since modeling feces transport is analogous to sediment transport, the movable-bed model is appropriate. However, feces do not fit the classic description of sediment for a variety of reasons. The particles are cohesive, larger than sand, and much less dense. Further complications arise from the relatively low flow rates and the surge characteristic of the discharge. Einstein (1944) notes that the time scale factor for sediment flow does not equal the time scale factor for water flow. He goes on to explain that the only way to establish the scale ratio for sediment flow is by data collection and analysis after the model is in operation. This is part of the frequently cited "artistic" stage of model verification.

The review that most completely addresses this situation is given by Henderson (1966) on pages 502-4. His movable-bed model design analysis is based upon Shield's threshold of particle movement, also presented in Henderson's treatise on pages 411-16. Shield bases his work upon shear stress at the bed interface, particle diameter, particle density, fluid viscosity, fluid density, fluid velocity, and gravity.

The entrainment function, F_s, and the particle Reynolds number Re* are the two dimensionless parameters used by Shield in sediment transport just as Froude and Reynolds number can be used for model studies. The aim, therefore, is to make F_s and Re* the same in the model and the prototype. Shield's plot of data on the F_s - Re* plane as presented on page 413 of Henderson (1966) is given in Appendix A. The state of the bed is determined by the position on the F_s - Re* plane. Although the conclusion is a tentative one, it has not been seriously contested since presented by Shield in 1936, especially for low values of the Froude number. In addition, the positions of both model and prototype in this study are well away from the critical region. Calculations are given in Appendix A.

Thus, use of Henderson's model analysis is appropriate for use in this study. The variables used are given in the List of Symbols and illustrated in Figure 1.

Henderson asserts that the Manning equation is valid for sediment transport. Also, Henderson states that the equivalent roughness will bear the same ratio

$A = W \times D_{max}$

$P = W + 2 \times D_{max}$

$R = A/P$

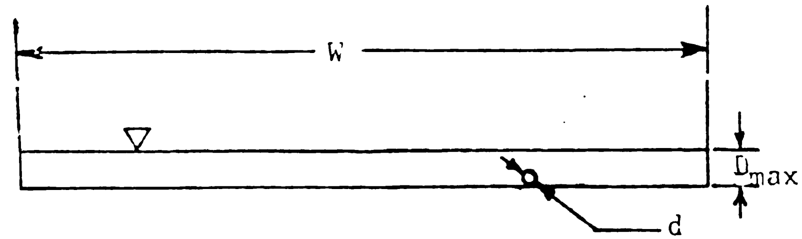

Section A-A

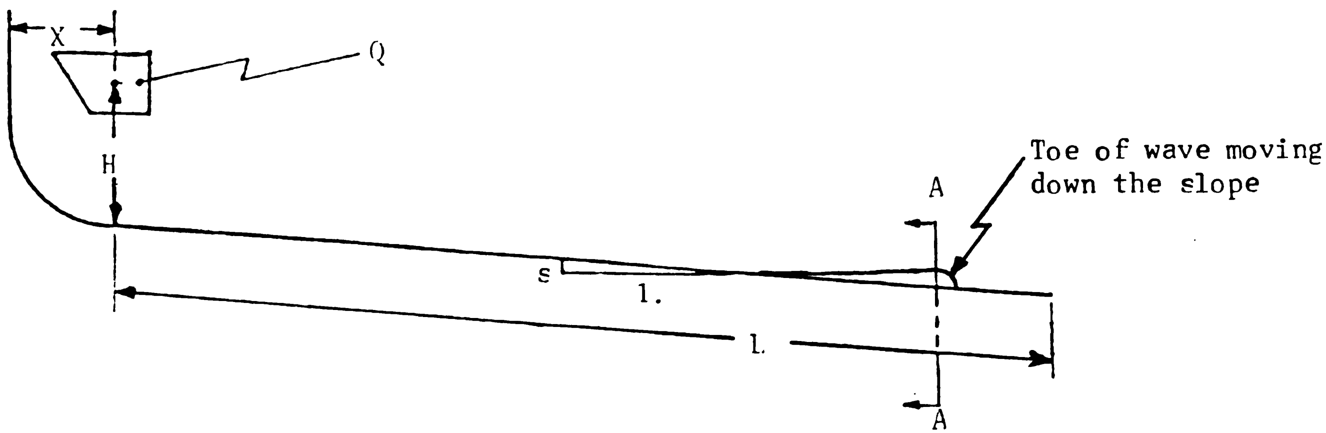

Figure 1.--Diagram of the flushing system showing some characteristic dimensions.

to the particle size in the model as in the prototype. This has two consequences: $n_r = d_r^{1/6}$, and $(R'/R'')_r = 1$. Thus:

$$n_r = d_r^{1/6} \qquad (1)$$

(Manning Equation)

$$v_r = \frac{R_r^{2/3}\ S_r^{1/2}}{n_r} \qquad (2)$$

(Slope)

$$S_r = Y_r/X_r \qquad (3)$$

(Froude No.)

$$v_r = Y_r^{1/2} \qquad (4)$$

(Velocity)

$$v_r = X_r/T_r \qquad (5)$$

(Discharge)

$$Q_r = v_r X_r Y_r = X_r Y_r^{3/2} \qquad (6)\ \text{from 4}$$

$$v_r = \frac{R_r^{2/3}\ Y_r^{1/2}}{n_r X_r^{1/2}} \qquad (7)\ \text{from 2 \& 3}$$

$$1 = \frac{R_r^{2/3}}{n_r X_r^{1/2}} \qquad (8)\ \text{from 4 \& 7}$$

Here, I have assumed that the hydraulic radius (R) is equal to the depth of flow (Y), making $R_r = Y_r$. For the shallow flows encountered in this flushing system, the error introduced is slight; the width-to-depth ratio minimum is 18. Shen (1971) states that "as a rule of thumb, for a width-depth ratio of larger than 10 in the model, no significant effect will be caused." Thus, the simplification is reasonable.

$$R_r = Y_r \tag{9}$$

$$n_r = d_r^{1/6} = \frac{Y_r^{2/3}}{X_r^{1/2}} \qquad \text{(10) from 1,8,9}$$

$$\left(\frac{R'}{R''}\right)_r = 1 \tag{11}$$

$$\begin{aligned} \tau_0 &= \tau_0' + \tau_0'' \\ &= \gamma A'S/P + \gamma A''S/P = \gamma R'S + \gamma R''S = \gamma RS \end{aligned} \tag{12}$$

$$(\tau_0)_r = \gamma_r R_r S_r = \gamma_r Y_r^{2}/X_r = Y_r^{2}/X_r \qquad \text{(13) from 3,9, 11,12}$$

Since water is used as a fluid in both model and prototype, $\gamma_r = 1$.

$$\alpha = S_s - 1 \tag{14}$$

(Entrainment Function)

$$F_s = \tau_0/\gamma(S_s - 1)d \qquad (15)$$

(Particle Reynolds No.)

$$Re^* = v^*d/\nu = (\tau_0/\rho)^{1/2}\, d/\nu \qquad (16)$$

$$1 = \frac{Y_r^{\,2}}{X_r \alpha_r d_r} \qquad (17)\ \text{from 13 \& 15}$$

$$1 = \frac{Y_r^{\,2} d_r^{\,2}}{X_r \nu_r^{\,2}} \qquad (18)\ \text{from 13 \& 16}$$

This leaves three equations (10, 17, 18) and five unknowns (d_r, Y_r, X_r, α_r, and ν_r). In Appendix B are data dealing with the viscosity (ν) of the flushing water as it flows down the alley acquiring sediment. The viscosity changes from about 1.1 cp to 2.0 cp as it acquires this sediment. The entrainment function (F_s) is not dependent upon ν, but the particle Reynolds number (Re^*) is inversely proportional to ν. From Shield's work presented in Appendix A, it can be seen that Re^*_m is not altered significantly when presented on the log scale for a change in ν by factors of less than 2.0. Re^* is well into the turbulent region. An explanation of model and prototype positions is presented in Appendix A. Therefore, the assumption that $\nu_m = \nu_p$ (or $\nu_r = 1$) is used to simplify the analysis by eliminating one of the unknowns. The equations are reduced to:

$$\frac{{Y_r}^2}{X_r \alpha_r d_r} = 1 \qquad (19)$$

$$\frac{{Y_r}^2 {d_r}^2}{X_r} = 1 \qquad (20)$$

$$d_r = \frac{{Y_r}^4}{{X_r}^3} \qquad (10)$$

$$1 = \frac{{Y_r}^2}{X_r \alpha_r d_r} = \frac{{X_r}^2}{{Y_r}^2 \alpha_r} \qquad (21) \text{ from } 10 \,\&\, 19$$

$$1 = \frac{{Y_r}^2 {d_r}^2}{X_r} = \frac{{Y_r}^{10}}{{X_r}^7} \qquad (22) \text{ from } 10 \,\&\, 20$$

$$1 = \left(\frac{{X_r}^2}{{Y_r}^2\ {}_r}\right)^5 \left(\frac{{Y_r}^{10}}{{X_r}^7}\right) = \frac{{X_r}^3}{{\alpha_r}^5} \qquad (23) \text{ from } 21 \,\&\, 22$$

or $X_r = {\alpha_r}^{+5/3}$

$$1 = \frac{{X_r}^2}{{Y_r}^2 \alpha_r} = \frac{{\alpha_r}^{10/3}}{{Y_r}^2 \alpha_r} \qquad (24) \text{ from } 21 \,\&\, 23$$

or $Y_r = {\alpha_r}^{7/6}$

$$d_r = \frac{Y_r^{\ 4}}{X_r^{\ 3}} = \frac{(\alpha^{7/6})^4}{(\alpha^{5/3})^3}$$

or (25) from 10,23,24

$$d_r = \alpha^{-1/3}$$

Thus, with three equations and four unknowns, the designer is free to choose one variable and the others will be fixed. The values proposed using Henderson's analysis and used in the design of the model are given in Table 1. Several of the parameters merit further discussion. The initial flush tank volume is based upon the bulk flow of water past a point, not on the length, width, and height scale factors. Both flush tank volume and channel roughness are often determined experimentally, the "artistry" stage of development. Particle density in this study is the apparent bulk specific gravity of the individual feces in water. Particle size was a perplexing problem in model scale down. Where Henderson (1966) calls for model particles to be larger than the prototype (d_r = 0.6867), Shen (1971) calls for model particles that are smaller than prototype size. Henderson's analysis for particle size is for river beds, but the flow conditions in this study are different. Due to the shallow flow, any increase in particle size, coupled with the decrease in flow depth (see vertical scale factor, Table 1) would change the

TABLE 1.--Initial modeling values.

Parameter	Prototype Value	Model Value	Scale Ratio
d	2.54 cm	3.71 cm	0.6867
Q	0.566 m^3	0.0118 m^3	47.09
R	4.80 cm	1.23 cm	
S	0.0236 m/m	0.0415 m/m	0.569
S_s	1.06176	1.020	
T^*	1 s	0.29 s	3.392
v	1 m/s	0.52 m/s	1.93
X : L	60.96 m	9.31 m	6.548
W	1.75 m	26.7 cm	6.548
Y : H	1.72 m	0.462 m	3.726
D	5.08 cm	1.36 cm	3.726
$\alpha = S_s - 1$	0.06176	0.020	3.088

*Time scale factor is based upon distance (L) and velocity (v) scale factors: $T_r = L_r/v_r$.

amount of particle submerged in the flow. This would greatly alter sediment transport characteristics in the model. To solve this inconsistency, I decided to verify the model first in fixed-bed mode (without sediment load). After fixed-bed verification, various sized particles would be inserted into the flow to find the correct particle scale factor. In this way, the model would be verified for movable-bed flow. Simultaneously, I could resolve the problem of sediment time scale differing from water time scale.

III. FIXED-BED PROCEDURE

Experimental Method

The model was constructed by gluing 9.5 mm plexiglass sheets together to form a long channel with vertical sidewalls. The channel is 9.31 m long, 26.7 cm wide, and the side walls are 14.3 cm high for the first 3.05 m, and 6.7 cm for the remaining 6.26 m. It rests upon a tubular support beam, made of 19.1 mm plywood. Each end is supported upon a table, which facilitates data collection and slope changes. Slope changes are effected by changing the support height under the input end. After set-up, a transit was used to check for sag: an insignificant 3.2 mm sag was detected. A carpenter's level is used to periodically check the direction perpendicular to flow, as wave channeling would result from an uneven bottom. At the inlet end, a sheet metal curve was constructed to direct the flow from the tip tank into the channel. The shape of the curve is approximately circular with radius of about 30 cm. The prototype curve shape is also approximately circular. I felt that distortion of the curve might significantly alter flow patterns when the tank dumped from low heights. The shape of the curve was deemed so important that distortion according to the modeling analysis was not followed. The dump tank is made of 12.7 mm plywood and rotates on a 2.54 cm pipe. The support for the tank is adjusted both horizontally and vertically so that the tank height and distance from the back wall above the curve can be changed. Dump volume is changed by two mechanisms. Styrofoam baffles of the same cross-section as the tank can be inserted so that the tank holds less water when it dumps and the water retains the same center of gravity. Also, weight in the form of washers and threaded nuts can be added to the front sloping side of the tank so the tank dumps sooner due to its shifted center of gravity.

The prototype system is located in the Finishing Building of the Michigan State University Swine Research Center. The building holds about 300 hogs, 20 to 70 kg in mass. Of the four flushed alleys, the one I chose to be the prototype was the second from the west wall of the building, adjacent to the center aisle. This alley is below the hog feeders for possible later study of feed build-up problems from leaky feeders. Also, at certain times of the year hogs will dung most frequently along the outside wall, creating non-uniform loadings in the two outside alleys. Thus, the two inside alleys are loaded more evenly. The alley is sloped 2.36% away from the dump tank and is 1.75 m wide. The tank dumps against a curved back wall that directs the flow down the channel. The side walls, alley floor, and lower portion of the curve are of concrete construction; the upper portion of the curve is sheet metal. It was constructed in 1970.

The flushing tank is constructed of 16-gauge steel sheet metal and reinforced at the corners and top with 50.8 mm × 50.8 mm × 3.2 mm angle iron. The bearing is mounted upon a 76.2 mm × 76.2 mm × 6.4 mm angle iron and rotates upon a 31.8 mm steel shaft. A sketch of the tank is shown in Figure 2. Fresh water was used for flushing in the fixed-bed model work.

The first step in model verification (fixed-bed analysis) involved simulation of the flow characteristics of the wave; no sediment transport was involved. The entrainment function and particle Reynolds number require two parameters of the flow to be modeled correctly: velocity and depth. Using the developments in the previous section, velocity and depth can be scaled as follows:

$$Y_r = 3.726$$

$$v_r = Y_r^{1/2} = 1.93 \text{ (Froude similarity)}$$

This required determining both the velocity and the depth of flow of the wave as it traveled down the alley. Both

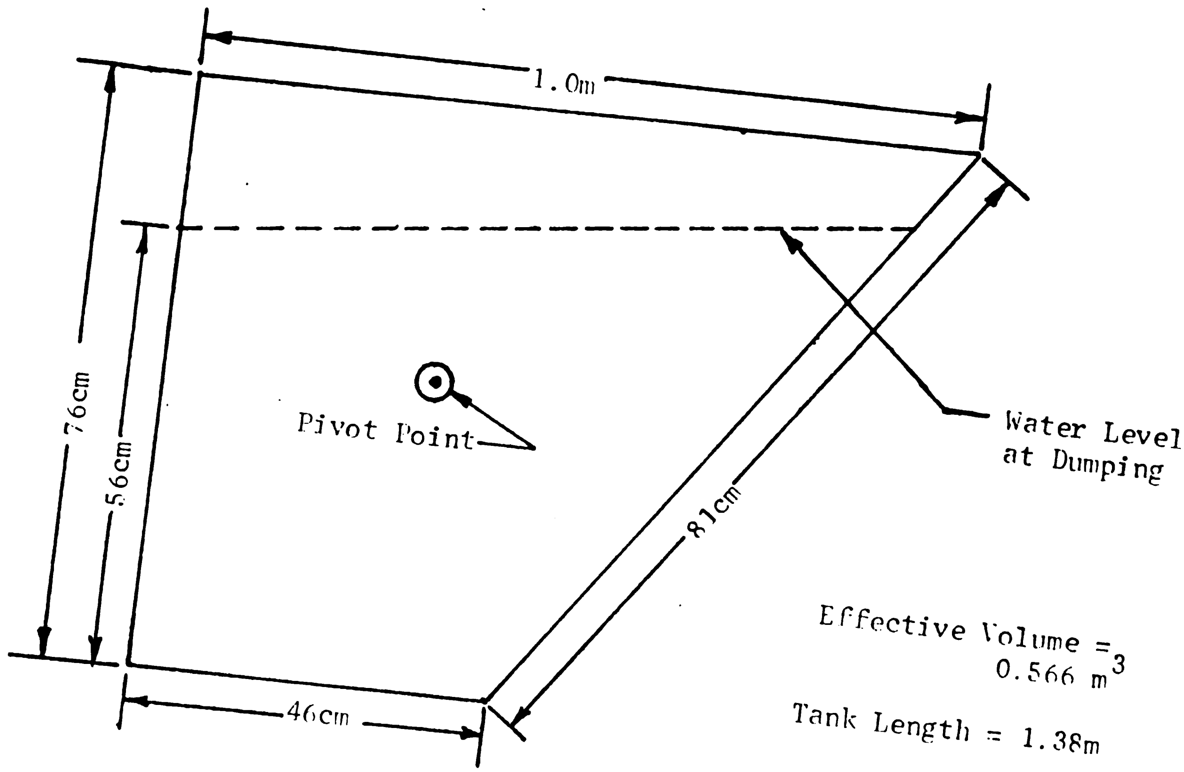

Figure 2.--The steel tank.

the prototype and the model were observed and recorded using a Bolex 16 mm movie camera running at 32 frames per second. Color film (Kodak 7241) was used due to the extremely long processing time for black and white film. Attempts to use videotape equipment were abandoned because the low frame speeds failed to stop the wave motion enough for data collection. The movie camera was stationed above and to the side of the flushed alley. Slats were lifted out, movie lights illuminated the alley, and an electric clock was positioned in the field of view. Distances and depths were inscribed on the sidewall opposite the camera. The alley was flushed several times prior to filming to completely clean it. When viewing the movie later for data collection, the picture included the wave passing, depth and distance markers, and an electric clock as a reference and a double-check on the running speed of the camera. Two distances from the dump tank were used, 14 m and 28 m as measured from the pivot point of the tank.

Data collection on both the model and the prototype consisted of frame-by-frame analysis of the movies. I took the depth directly from the film and calculated velocity using the distance traveled and the running speed of the film (32 frames per second). The distance that the wave traveled from one frame to the next proved to be difficult to determine. The clear fluid did not provide enough reference objects to observe the distance changes. At first, small surface waves and surface bubbles were used as guides. However, inconsistent data were obtained. I used a stroboscopic light source, a Polaroid camera, and small particles inserted into the flow in the model to determine flow velocities at different depths of the wave. Four to seven strobe flashes per photograph clearly indicated that velocities at different depths were significantly different. The particle velocities near the top of the wave were on the order of 20% greater than the particle velocities near the bottom. Thus, to accurately correlate the velocity from prototype to model, buoyant objects had to be used in the flow as reference points. It was important that the particles were the same height in the wave in each case, thus the wave surface was chosen. Marshmallows and chocolate malt balls were used in the prototype and dired peas and white beans in the model, both due to their color, biodegradable characteristics, and relative sizes as compared with flow depth. The assumption that these particles moved at the same velocity as the water is valid until flow becomes shallow and the particles start to roll instead of float, at which point data collection stopped.

The validity of measuring velocities with tracer particles was verified in the model by inserting the particles in a steady-state flow condition. Discharge as calculated using particle velocity, flow depth and channel width was within 2% of actual discharge.

As one particle passed from view on the film, another particle was chosen and followed until it either became obscure or passed from the screen also. A continuous reading of velocity was thereby possible. Also, the distances that each of the individual particles traveled was summed to give a total distance of water passage past the point of observation. Graphs were drawn of velocity and depth versus cumulative distance of water past the observation point. If after proper scaling of the model data, the model curve was identical to the prototype curve, then model verification in the fixed-bed stage would be complete. This is very exacting criterion for verification. In effect, the entire wave shape and time of passage must be reproduced by the model in order to complete the verification process.

Results and Discussion

Flushing events were filmed both in the swine barn (prototype) and using the model. An initial set of data are presented in Figures 3 and 4. The ordinate on these graphs is depth or velocity of the surge wave.

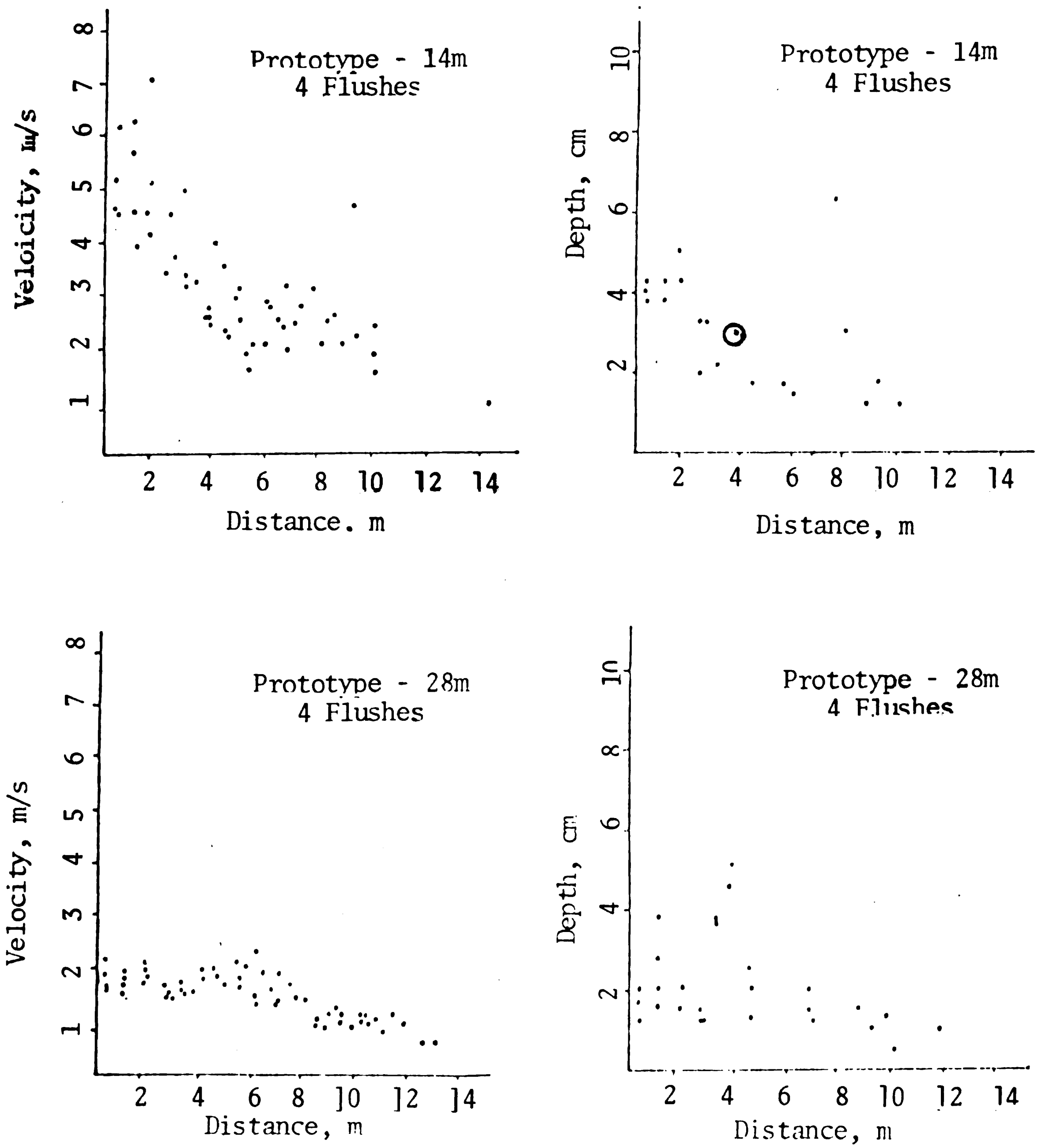

Figure 3.--Velocity and depth measurements for the prototype at 14 and 28 meters from the dump point.

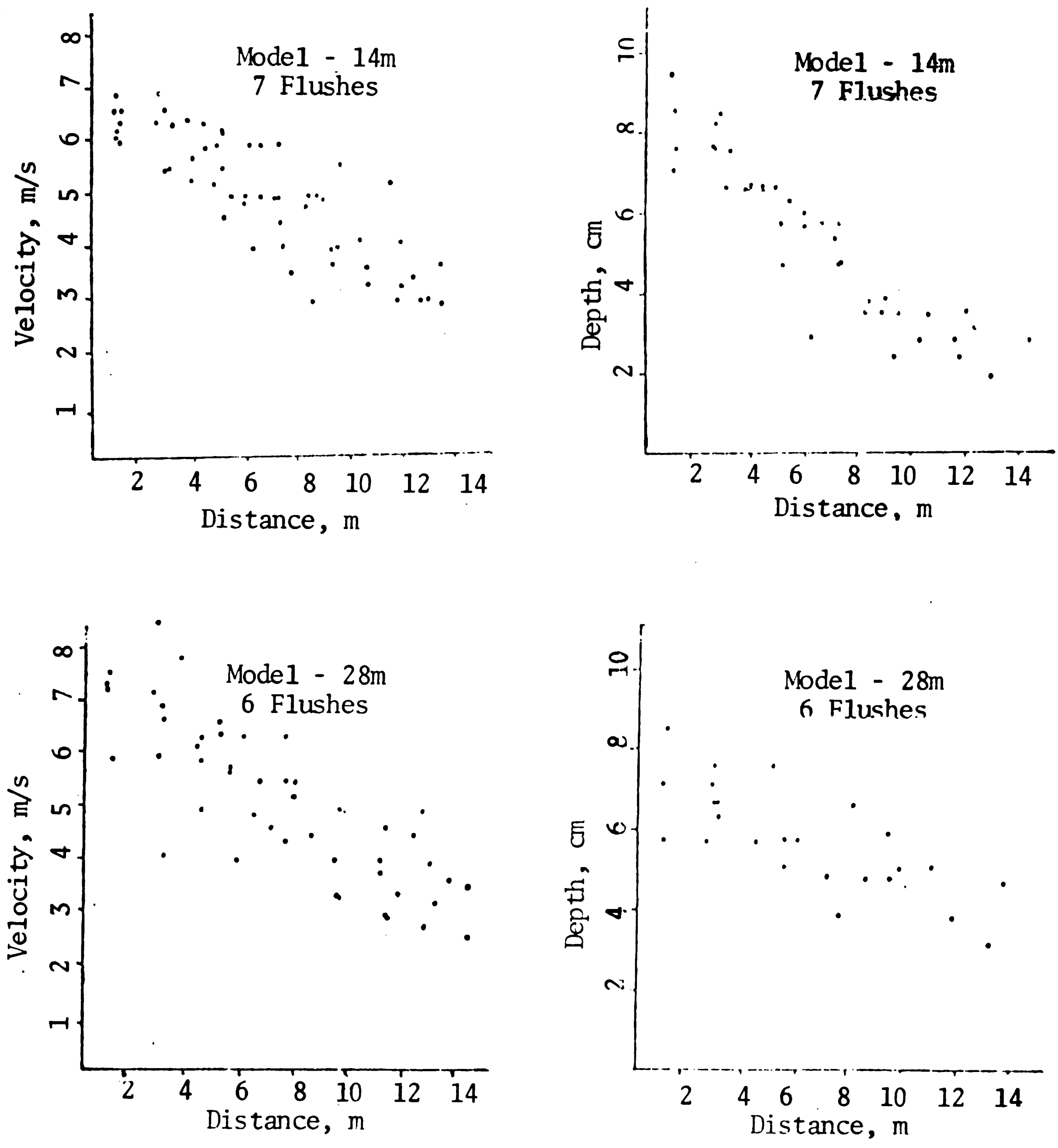

Figure 4.--Velocity and depth measurements for the model at 14 and 28 meters from the dump point.

As explained earlier, depth readings were taken directly from the film. Velocity readings were calculated using the distance traveled by the tracer particles, the number of frames of film that were exposed during this travel, and the running speed of the film (32 frames per second). The abscissa is the length of water which has passed the observation point, a more difficult concept to understand. For example, examine the circled data point in the upper right-hand graph of Figure 3. To place this point, the two values of depth and distance must be found. Depth was read directly from the film, about 3 cm. Distance, or the length of water past the observation point, was calculated by summing the distance of travel of each tracer particle followed. The observation point was fixed, in this instance at 14 m. As each particle passed from view or became obscure, the distance it had traveled since I had started to follow it was recorded. I then selected another tracer particle to follow and the process was repeated. For this example, when the flow depth had reached 3 cm, particle distances summing to 4 m had passed the observation point. In addition to summing them for a total distance, the individual distances were used for calculating average velocities for that seciton of flow.

The scatter in the data can be partially explained by the difficulties encountered in reading the films. At the toe of the wave, there is a good deal of turbulence and the accuracy of tracing the wave front (velocity) can be in error as much as 20%. Tracer particles shortly behind the wave front are sometimes blurred even at 32 frames per second. Moreover, there is a velocity gradient with depth of flow. Particles near the sidewall were ignored. Thus, the scatter in the data at the toe of the wave is unavoidable. Just after the wave crest has passed the observation point, velocity measurements are much more accurate due to decreased turbulence. The uncertainty later in the flow arises from the possible accumulation of error in estimating the total distance of water which has cumulatively flowed past the observation point. This may amount to about 5% error near the end of the wave.

From Figures 3 and 4, one can see that model velocity approximately mimics prototype velocity at 14 meters from the dump tank's pivot point. At 28 meters, however, the model gives velocities which are too high. Reasons for the discrepancy may be tip tank volume and surface roughness. As can be seen from the data, the depth of flow in the model is too great, leading me to believe that the volume used in the model was too great.

Entering the artistry stage of the model development, I chose to do a series of tests combining several volumes, and an additional surface roughness. Data presented in Figures 5 and 6 represent the optimum data sets. The volume of water dumped was decreased to 40% and 30% of the original volume dumped for these two tests. Surface roughness was increased by attaching randomly creased aluminum foil to the surface. Figure 5 gives the model data for 40% volume and Figure 6 gives the model data for 30% volume. I chose to use 35% of original volume flushed as the new volume in the model as this was a good compromise between the two. To quote Shen (1971):

> This is where modeling becomes an art as well as where much unjustifiable discredit to the technique enters . . . a distorted model is a compromise between a number of requirements . . . but only upon trial and error will one be able to find the best compromise.

The corrected flush volume increased the flush volume scale ratio from 47.09 to 134.5, closer to the value of 159.8 obtained from length, width, and height scale factors. The reason why a decrease in volume was necessary was not clearly understood.

Studies near the end of the model verification process have since indicated that the volume of the water flushed should be modeled statically rather than dynamically. This would correspond to a flush volume of 30% of the original flush volume in the model. Also, roughness should be increased with distance from the dump tank. It appears from data collected that the addition

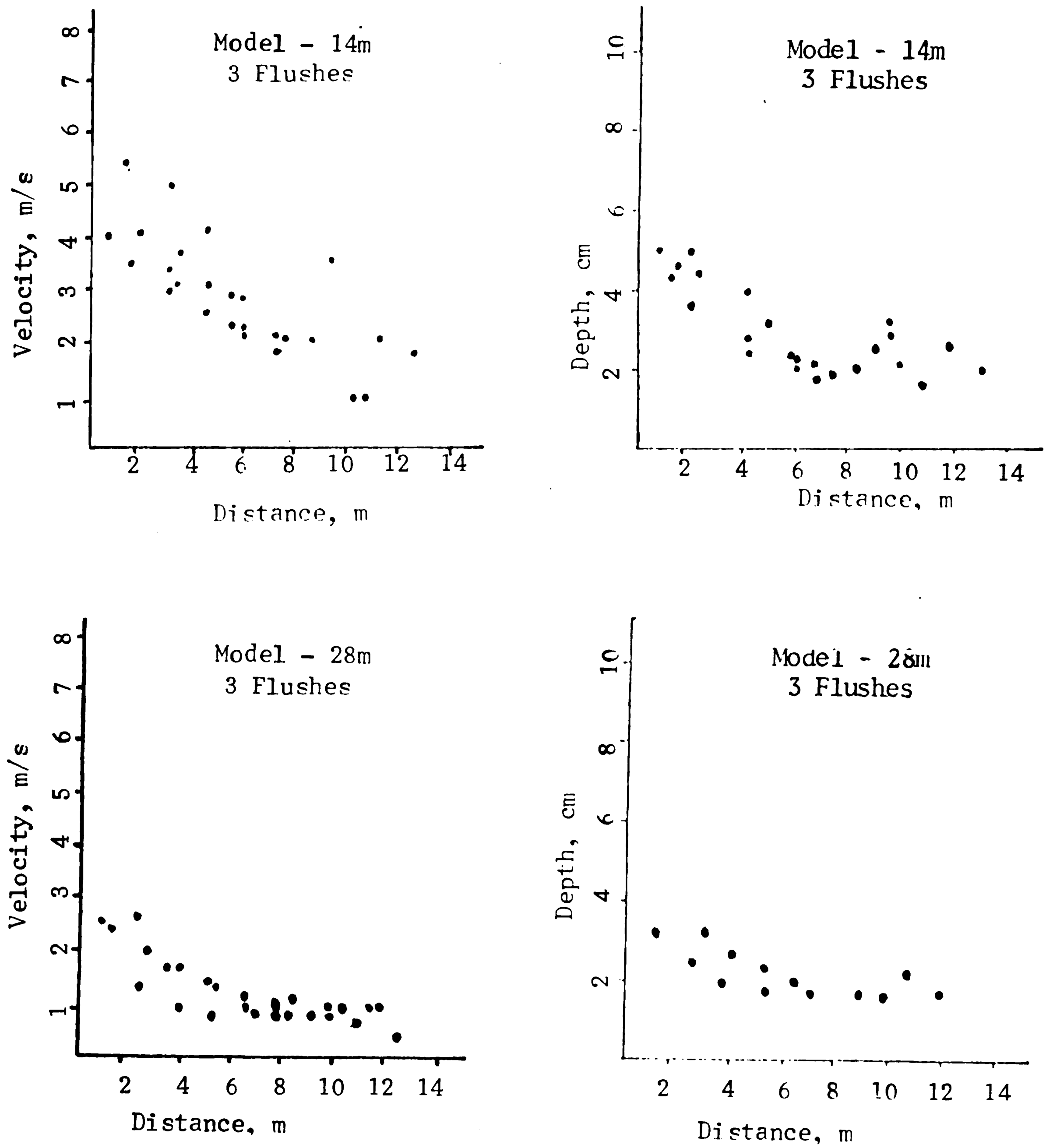

Figure 5.--Model velocity and depth data at 14 m and 28 m from the dump point. Volume has been reduced to 40% of original dump volume.

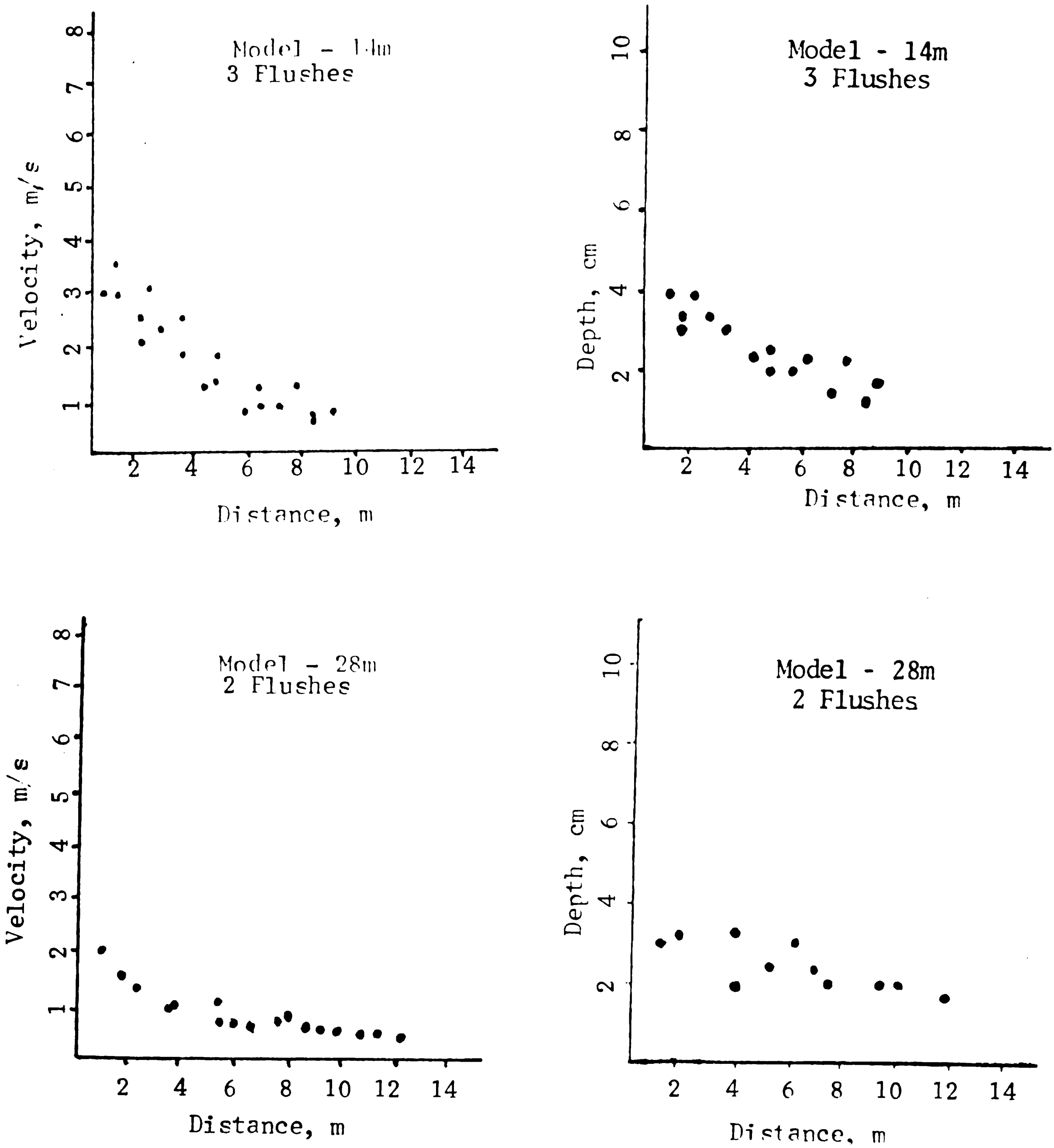

Figure 6.--Model velocity and depth data at 14 m and 28 m from the dump point. Volume has been reduced to 30% of original dump volume.

of the aluminum foil to the model surface should start at approximately 50 meters (8 meters on the model) from the dump tank. This change would not significantly alter the performance of the model from what it was during the movable-bed tests which were based on 35% of the original flush volume and constant roughness.

Also, during this phase of the study, I conducted a small experiment on the model relating tip tank position to water turbulence on the dump curve and kinetic energy in the wave. Turbulence was roughly measured by taking films of dye being injected into the stream as it was flowing over the dump curve. The relative width of the dye bands gave an indication to the turbulence present on the curve. A rough estimate of the kinetic energy of the wave after passing through the curve was obtained by its average velocity down the channel. As could be expected, both the turbulence on the curve and the energy of the wave after the curve increased as the tank was raised. A more interesting phenomenon occurred when the tank was moved away from the back wall at the various heights. As the tank was moved away from the wall, the turbulence on the curve generally increased and the energy in the wave generally decreased. Both of these indicate that the optimum position for a tip tank of this nature is as close to the back wall as possible. The probable reason for this is that the water can "attach" to the wall and curve easier at a larger angle of incidence, resulting in less turbulence and energy loss.

Another interesting phenomenon was that during the flow in both the prototype and the model a second surge of water passes down the channel shortly behind the wave toe. (This causes some of the scatter in the data in Figures 3-6.) This "second wave" is not nearly as pronounced as the initial wave, but is important none-theless.

It is hypothesized that the cause of this second wave is the tipping nature of the tank. As the tank rotates, some water may be "caught" in the tank bottom due to "centrifugal force." This water doesn't leave the tank until it is almost fully rotated. Then it causes a second surge when it is released onto the curve.

IV. MOVABLE-BED PROCEDURE

Experimental Method

After verification of the model in fixed-bed mode, the next step in the development process was movable-bed verification. This consisted of adding various sized particles to the flow in the model and determining which size mimicked the particles inserted into the flow in the prototype. The criterion used was the mean flushed distance of several flushes. Particles were all the same shape, that of a cube with spherical corners. Particles (henceforth termed Standard Energy Abosrbers, or S.E.A.) used in the prototype were molded with a resin-hardener mixture. S.E.A. used in the model were made from various sized wooden spheres by sawing six flat perpendicular faces. All S.E.A. were adjusted to a specific gravity of 2.1 by adding a core of lead.

A new fiberglass tank was constructed and used in data collection. I chose a fiberglass construction due to its rust-resistant property. The pivot point of the tank could be moved to alter the volume of water released. Telescoping supports were used to permit varying tank height and distance from the back wall. Several positions and volumes could be checked on both the prototype and the model. There were two modifications in design of the tank compared with the previously used steel tank. Since the new tank was made of fiberglass, the stops that the steel tank rested on during filling and hit against to prevent excess rotation during dumping had to be eliminated. The fiberglass would not have withstood the impact. This change required the tank shape to be altered slightly. In the fiberglass tank the front side slopes much more steeply. (See Figure 7.) It was necessary to make a stopless tank more symmetric so that it would fill nearly full prior to dumping. If the front side extends too far from the center of the tank, three events may take place: (1) the tank may dump backwards partially full, (2) the tank may dump forward partially full, or (3) the tank may overflow without tipping. These events, of course, depend upon pivot point location; the point is that there may not be a location that allows the tank to fill and then dump using the older tank shape. The greater moment resulting from a greatly extended front is hard to control in a stopless tank.

The tank was constructed by applying alternate layers of resin and fiberglass matting to the outside of a wooden mold. The mold was constructed with at least 2° draft on all sides and was planed, sanded, painted, and waxed to facilitate removal of the tank when dry.

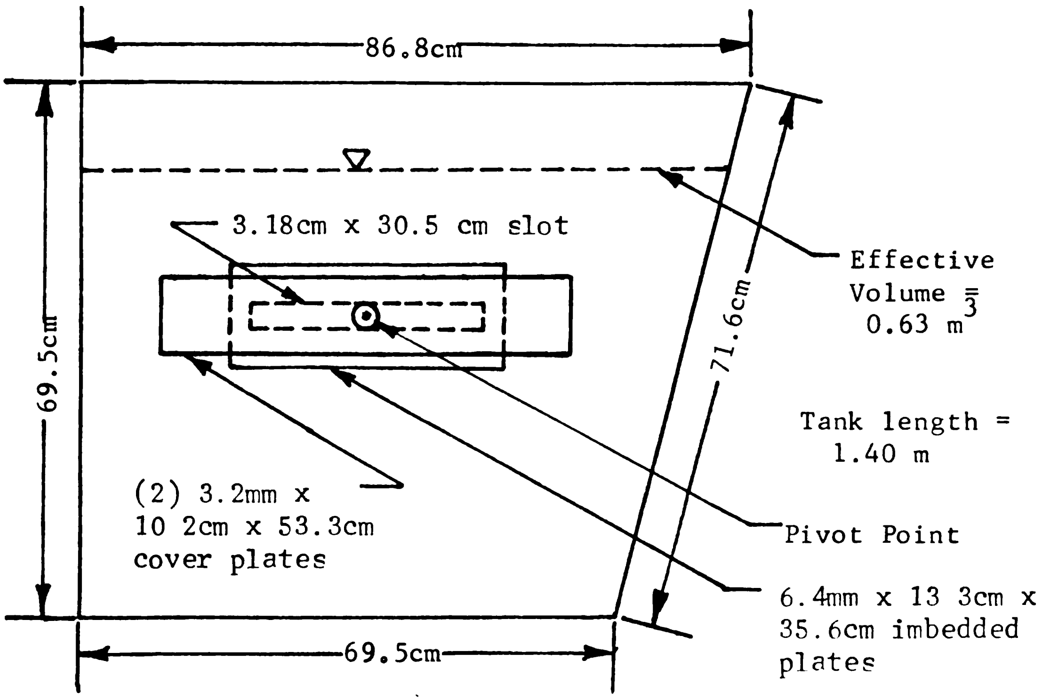

Note: Pivot Point is located 39.4cm from tank bottom and 37.5cm from the back wall .

Figure 7.--The fiberglass tank.

There were two layers of fiberglass matting in the tank with two extra layers on the ends. Between the layers, there was a sheet metal frame for extra support at the corners and top. Welded to this frame on each end was a 6.4 mm steel plate to carry the bearing load from the tank to the 3.18 cm shaft on which the tank rotates. The plate had a horizontal slot 30.5 cm × 3.18 cm for pivot point adjustment. Telescoping supports consisted of three different sizes of steel pipe that closely fit within each other. Holes drilled for 1.27 cm diameter pins allowed for tank position adjustment. The bearings were mounted on a horizontal plate at the junction of the supports.

Results and Discussion

Data were collected on the prototype as follows. Five S.E.A. were placed across the alley about 3 m from the dump tank. After one flush, I measured the distance each S.E.A. was flushed. Depending upon tank position and volume, two or three dumps were required to flush the S.E.A. the 30 m to the opposite end of the prototype. Data from each flush were recorded. Dumps were replicated thrice for each tank position and volume, making a total of 15 data points in each set (five S.E.A. per dump for three dumps). Distances were measured from the pivot point location closest to the back wall; the end of the continuously sloped section was 31 m from the pivot point. Data past this point were questionable; S.E.A., however, never reached this point with the first dump. Although the data from the second and third dumps were recorded, they were not used in determining the particle scale factor. The data collected are presented in Table 2, along with the model data.

Model data were obtained by essentially the same method. However, since only one S.E.A. of each size was flushed each time (for a total of four per dump), 15 dumps were required at each tank position and volume to obtain a data base of 15 per set.

From the data presented, one can visually determine a range for the particle scale ratio. Approximate scale ratios are given for each tank position and volume. These were determined by comparing the mean distance flushed for the prototype with the corresponding values for the four model S.E.A. The prototype value falls somewhere in the range or just outside the range of model values. Each model S.E.A. has a particle scale ratio value, obtained by dividing the prototype S.E.A. diameter by that particular model S.E.A. diameter; these are also given in Table 2. An approximate particle scale ratio can then be obtained by comparing the location of the prototype-model intersection with the particle scale ratios.

TABLE 2.--Standard Energy Absorbers data. (Numbers represent mean distance flushed (m) with one dump.)

Prototype Position				Model S.E.A.				
Height (m)	Distance to wall from pivot point (m)	Prototype Volume (m^3)	Prototype S.E.A.	#1	#2	#3	#4	Approx. Scale Ratio
1.562	0.711	0.630	23.72	17.37	20.73	25.91	26.52	1.9
1.562	0.711	0.580	22.53	13.19	16.19	21.74	23.00	2.2
1.562	0.711	0.485	19.77	10.04	12.76	16.76	16.32	2.8
1.778	0.648	0.576	24.12	12.40	16.09	20.81	23.23	2.3
1.778	0.648	0.501	20.72	10.59	12.27	19.51	20.30	2.3
1.778	0.648	0.427	19.10	9.59	12.09	17.72	17.84	2.4
1.791	0.883	0.515	22.70	12.37	15.16	22.70	23.98	2.2
1.854	1.067	0.515	20.36	12.07	13.38	17.89	19.63	2.3
1.930	0.756	0.551	22.15	10.34	11.95	19.53	21.36	2.3
1.956	0.953	0.551	21.70	12.21	14.59	21.28	21.74	2.2
1.911	0.660	0.551	22.44	11.20	13.35	17.62	17.84	2.8
1.911	0.660	0.399	18.69	9.98	11.62	15.16	17.46	2.4
1.911	0.660	0.576	23.61	15.24	16.99	23.30	24.22	2.2
Particle diameter scale ratios				1.46	1.57	2.15	2.22	

The range of particle scale ratios was 1.9-2.8. Ten of the 13 values fall in the range of 2.2-2.4. For the complete sample set of 13 values, the sample mean was 2.33 and sample standard deviation was 0.24. The mean and standard deviation of the sample minus the two 2.8 values were 2.25 and 0.14, respectively. In addition, subtracting the 1.9 values gives $\bar{x} = 2.28$ and $s = 0.079$. Thus, the values suggest a strong possibility of the true value for the ratio falling in the range of 2.2-2.4. For this reason, 90% and 95% confidence intervals were calculated for the total data set (13 values):

	Lower Limit	Upper Limit
90%	2.21	2.45
95%	2.18	2.48

Thus, I conclude that the range for the particle diameter ratio is 2.2-2.5. The most probable exact value for the ratio is 2.3.

I used the Buckingham π Theorem to obtain a dimensionless parameter that might explain the particle diameter scale ratio. I combined these dimensionless parameters to obtain new dimensionless parameters. Through cancellation of dimensioned parameters, one particular dimensionless parameter reoccurred several times. The particular parameter was a modification of the Froude number (Fr*), $(v^*)^2/dg$, where v^* is the shear velocity (see Shield's threshold of movement work, outlined in

Appendix A). The Froude number is very important in open-channel flow, and this modification includes the particle diameter and the shear at the bed.

Since the object is to make Fr* equal in the model and the prototype,

$$\frac{(Fr)_p}{(Fr)_m} = (Fr)_r = 1.0 = \frac{(v*_r)^2}{d_r g_r}$$

$$g_r = 1.0, \quad \therefore \quad d_r = (v*_r)^2$$

From Appendix A,

$$(v*)_r = \frac{(v*)_p}{(v*)_m} = \frac{0.1054 \text{ m/s}}{0.06869 \text{ m/s}} = 1.53$$

$$d_r = (v*_r)^2 = (1.53)^2 = 2.34$$

This value corresponds to the value of 2.3 obtained using the S.E.A. approach and is thus a possible explanation.

Final modeling values used in the verified model are given in Table 3.

One point I would like to make here is the importance of the tank position relative to the floor and wall. The tank axis must be perfectly parallel to both the wall and floor. At one point, I found that I could strongly influence the distance that the S.E.A. were flushed in

TABLE 3.--Final modeling values.

Parameter	Prototype Value	Model Value	Scale Ratio
d	2.54 cm	1.1 cm	2.3
Q	0.566 m^3	0.004133 m^3	134.5
R	4.80 cm	1.16 cm	
S	0.0236 m/m	0.0415 m/m	0.569
S_s	1.06176	1.020	
T^*	1 s	0.29 s	3.392
v	1 m/s	0.52 m/s	1.93
X : L	60.96 m	9.31 m	6.548
W	1.75 m	26.7 cm	6.548
Y : H	1.72 m	0.462 m	3.726
D	5.08 cm	1.27 cm	4.00
$\alpha = S_s - 1$	0.06176	0.020	3.088

*Time scale factor is based upon distance (L) and velocity (v) scale factors: $T_r = L_r/v_r$.

the model by where I placed them in the channel. It seemed that near the dump curve (where the S.E.A. were placed) the depth of flowing water was greater on one side than the other, even though both the flume and curve were level and square. The cause of the problem was that the tank itself was not level. This caused the water to have a slightly askew velocity as it was dumped onto the curve. After approximately one meter in the model, the wave profile had returned to normal. However, the first surge of flow on the deeper side imparted enough momentum to the S.E.A. on that side to often transport them farther than the others. Thus, the tip tank must be level and square with the wall for best performance.

V. SUMMARY AND CONCLUSIONS

A distorted, movable-bed model was constructed to simulate hydraulic transport of livestock feces. The verification process consisted of three phases: model construction, fixed-bed verification, and movable-bed verification. Each is summarized below.

The model was constructed of plexiglass, with a wooden tank and wooden tubular support. The curve was made of sheet metal. The size of the model was determined by values derived from Henderson's model analysis which was based upon Shield's threshold of sediment movement work. The distorted model thus obtained had a horizontal scale ratio of 6.548 and a vertical scale ratio of 3.726.

Fixed-bed verification (no sediment load) consisted of fine-tuning the model for flushing wave depth and velocity at 14 m and 28 m from the dump tank. I analyzed movie film frame by frame to determine velocities and depths. Small buoyant particles inserted in the flow aided in velocity readings. To obtain the correct flow characteristics in the model, the flush volume was reduced to 35% of Henderson's recommendation and surface roughness was increased by attaching a sheet of randomly creased aluminum foil.

Verification of the model in the movable-bed state (sediment load) required the correct scaling of the particle diameter. I used a cube with rounded corners (termed "Standard Energy Absorber") adjusted to a specific gravity of 2.1 in both the prototype and model. Different sized S.E.A. in the model were compared with the prototype S.E.A.; mean flushed length was the criterion. The particle diameter scale ratio was determined to be in the range 2.2 to 2.5.

A dimensionless parameter (Fr*) was proposed as a possible explanation for the particle diameter scale ratio of 2.3.

Additional conclusions are that the dump tank must be level, square to the wall, and as close as possible to the wall to be most efficient. Also, I found that the kinematic viscosity of the flushed water changes from 1.1×10^{-6} to 2.0×10^{-6} m^2/s in the wave as it traveled down the alley.

APPENDICES

APPENDIX A

SHIELD'S WORK AS PRESENTED IN HENDERSON

APPENDIX A

SHIELD'S WORK AS PRESENTED IN HENDERSON

Figure 8 is Shield's plot of the entrainment function, F_s, against the particle Reynolds number, Re*. The region on the left side represents laminar flow, the center section is the transition region or threshold of movement at the bed, and the section to the right corresponds to turbulent flow and sediment transport at the bed. The sediment load increases as one proceeds upward on the plot and full suspension of sediment is reached at $F_s \approx 0.6$. Since bed formation is determined by position on the F_s - Re* plane, model position must correspond to prototype position. However, in this case, a slightly less vigorous criteria is acceptable. If both model and prototype are well into the turbulent region of flow and suspension of sediment is possible, the model will mimic the prototype for sediment transport, the parameter of interest. Thus, all values of F_s greater than 0.6 indicate equivalent bed states, that of full sediment suspension. A similar argument can be applied to Re* values. The turbulent region of flow at the bed is indicated on the graph where the curve levels

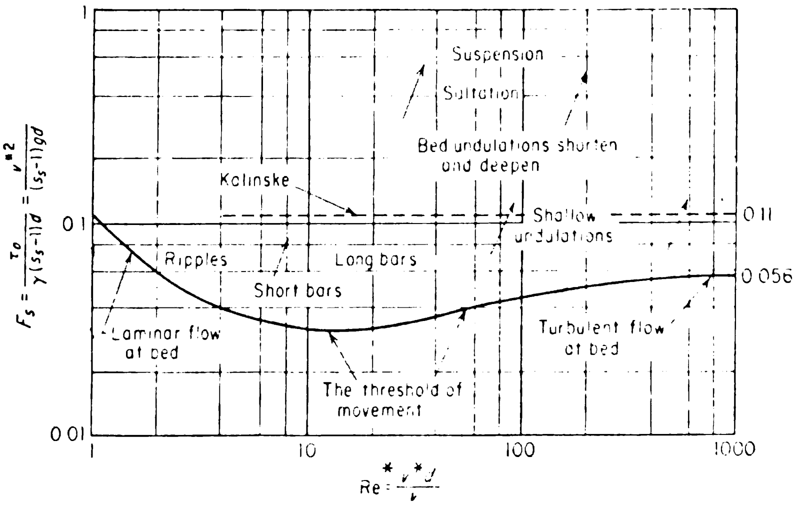

Figure 8.--The entrainment function, after A. Shields.

out and F_s becomes constant. This indicates that similar flow conditions at the bed are indicated by all values of Re* above 500.

Values of F_s and Re* are calculated as follows:

$$Re^* = \frac{v^*d}{v}$$

$$F_s = \frac{(v^*)^2}{gd(S_s-1)}$$

$$v^* = \left(\frac{\tau}{\rho_f}\right)^{0.5}$$

$$\tau = \gamma RS$$

τ_0 = the shear stress at the bed, kg/m-s^2

ρ_f = the fluid density, kg/m^3

g = the acceleration of gravity, m/s^2

v^* = the "slear velocity," m/s

d = the particle diameter, m

ν = the fluid kinematic viscosity, m^2/s

S_s = the specific gravity of the particles, unitless

γ = the density of the fluid × gravity (ρg), kg/m^{2}s^2

R = the hydraulic radius of flow, m

s = the slope of the channel, m/m

Computation of Significant Parameters for the Prototype

$$\gamma = \frac{10^3 \text{ kg}}{\text{m}^3}\,\frac{9.8 \text{ m}}{\text{s}^2} = 9.8 \times 10^3 \text{ kg/m}^2\text{s}^2$$

R (at wave crest) width = 1.7526 m (69 in)

depth = 0.0508 m (2 in)

$$R = \frac{wd}{2d + w} = \frac{0.0890 \text{ m}^2}{1.3542 \text{ m}} = 0.0480 \text{ m}$$

S = 0.0236 m/m

S_s = 1.06176

ν = 1.1 to 2.0 ct (for ρ = 1.0 gm/cm^3, 1ct = 1cp) (see Appendix B).

Take 1.5 ct = 1.5 × 10^{-6} m^2/s as the average.

d = 2.54 cm = 0.0254 m (1.0 in)

$$g = 9.8 \text{ m/s}^2$$

$$\rho_f = 1.0 \text{ g/cm}^3 = 10^3 \text{ kg/m}^3$$

$$\tau = \gamma RS = \frac{9.8 \times 10^3 \text{ kg}}{\text{m}^2\text{s}^2} \left| \frac{0.048 \text{ m}}{} \right| \frac{0.0236 \text{ m}}{\text{m}}$$

$$\tau = 11.1 \text{ kg/ms}^2$$

$$\nu^* = \left(\frac{\tau}{\rho_f}\right)^{0.5} = \left(\frac{11.1 \text{ kg/ms}^2}{10^3 \text{ kg/m}^3}\right)^{1/2} = 0.1054 \text{ m/s}$$

$$Re^* = \frac{v^* d}{\nu} = \frac{(0.1054 \text{ m/s})(0.0254 \text{ m})}{1.5 \times 10^{-6} \text{ m}^2\text{s}} = 1.784 \times 10^3$$

$$F_s = \frac{(v^*)^2}{gd(S_s - 1)} = \frac{(0.1054 \text{ m/s})^2}{(9.8 \text{ m/s}^2)(0.0254 \text{ m})(0.06176)}$$

$$F_s = 0.7226$$

This position, although not an exact one, is clearly into the turbulent fully suspended region on Shield's plot.

Model Parameters

$$\gamma = 9.8 \times 10^3 \text{ kg/m}^2\text{s}^2$$

$$R = \frac{wd}{2d + w} \quad \begin{array}{llr} \text{[depth} & 0.0127 \text{ m} & \text{(0.5 in)]} \\ \text{[width} & 0.2667 \text{ m} & \text{(10.5 in)]} \end{array}$$

$$= 0.0116 \text{ m (9.7\% error)}$$

$$S = 0.0415 \text{ m/m}$$

$$S_s = 1.02$$

$$\nu = 1.20 \text{ ct} = 1.2 \times 10^{-6} \text{ m}^2\text{s (tapwater at 13°C)}$$

$$d = 0.01 \text{ m}$$

$$g = 9.8 \text{ m/s}^2$$

$$\rho_f = 1.0 \text{ g/cm}^3 = 10^3 \text{ kg/m}^3$$

$$\tau = \gamma RS = \frac{9.8 \times 10^3 \text{ kg}}{\text{m}^2\text{s}^2} \left| \frac{0.0116 \text{ m}}{} \right| \frac{0.0415 \text{ m}}{\text{m}}$$

$$= 4.718 \text{ kg/ms}^2$$

$$v^* = \left(\frac{\tau}{\rho_f}\right)^{0.5} = \left(\frac{4.718 \text{ kg/ms}^2}{10^3 \text{ kg/m}^3}\right)^{0.5} = 0.06869 \text{ m/s}$$

$$Re^* = \frac{v^*d}{\nu} = \frac{(0.06869 \text{ m/s})(0.011 \text{ m})}{(1.2 \times 10^{-6} \text{ m}^2/\text{s})} = 629.$$

$$F_s = \frac{(v^*)^2}{gd(S_s-1)} = \frac{(0.06869 \text{ m/s})^2}{(9.8 \text{ m/s}^2)(0.011 \text{ m})(0.02)} = 2.19$$

The model is also well into the turbulent, fully suspended range on Shield's plot. This confirms the model as correctly portraying the turbulent, sediment carrying situation that exists in the prototype. Both model and prototype have values of F_s greater than 0.6 and Re* greater than 500.

APPENDIX B

VISCOSITY OF FLUSHING WATER

APPENDIX B

VISCOSITY OF FLUSHING WATER

Kinematic viscosity (ν) of the flushing water is an important factor in the sediment transport capacities of the water. Also, the particle Reynolds number (Re*), which is one axis of Shield's plot in the model analysis, is inversely proportional to ν. Thus, measurements were required to determine if the viscosity of the recycled lagoon water used for flushing was sufficiently close to water for the model analysis. The kinematic viscosity of water used in the model is 1.2×10^{-6} m^2/s at well temperature, and the assumption made in the model analysis was that the model water viscosity would equal the flushing water viscosity. Thus, the flushing water must be sufficiently close to this value to warrant this assumption. Water samples were taken from the tank just before dumping. Samples were also collected at the opposite end of the alley after a typical dump. This was done by holding a sample jar at the end of the alley and sampling the wave front as it passed. The front contains the highest solids loading and would thus be the "worst case." A rotary model LVF Brookfield viscometer was used for measurements. To increase the degree of sensitivity of the meter, a large hollow cylinder was attached to a spindle. This increased the surface area in contact with the sample, requiring a larger torque to maintain its rotation in the sample. Data are given below:

Trial 1: Sample Taken From Wave Front

T = 22°C for all samples

Spindle Speed (rpm)	Tap Water (Std.)	Pre-flush Water	Post-flush Water
12	20.4, 20.7, 20.5	--	40.9, 41.9, 42.5
($\bar{X}$)	20.5	--	41.8
30	79.0, 87.2, 85.8	92.6, 89.9, 94.1	--
($\bar{X}$)	84.0	92.2	--

Using water as the Standard:

$$\text{Pre-flush water} = \frac{92.2}{84.0}\,(1.0 \times 10^{-6}\ m^2/s) = 1.1 \times 10^{-6}\ m^2/s$$

$$\text{Post-flush water} = \frac{41.8}{20.5} = 2.0 \times 10^{-6}\ m^2/s$$

Trial 2: Sample Taken Just Past Wave Front

Spindle Speed (rpm)	Tap Water (Std.)	Pre-flush Water	Post-flush Water
12 ($\bar{X}$)	22.0	25.3	30.0
30 ($\bar{X}$)	83.0	90.0	--

Pre-flush water = $\frac{90}{83}$ $(10.0 \times 10^{-6}\ m^2/s) = 1.1 \times 10^{-6}\ m^2/s$

or

$\frac{25.3}{22.0}$ $(1.0 \times 10^{-6}\ m^2/s) = 1.1 \times 10^{-6}\ m^2/s$

Post-flush water = $\frac{30}{22}$ $(1.0 \times 10^{-6}\ m^2/s) = 1.4 \times 10^{-6}\ m^2/s$

Thus, the kinematic viscosity of the water in the wave changes as it acquires solids from 1.1 to $2.0 \times 10^{-6}\ m^2/s$ in the wave front and less later in the wave. To answer the question of how drastic a change this is, one must look at Shield's plot in Appendix A. It was shown there that the particle Reynolds number and the entrainment function are both well into the turbulent region of the plot, as would be expected. On the log scale, a change in the Re* by a factor of two does not affect the model position greatly. In fact, the change is away from the critical transition area of the plot. As was stated earlier, the degree of turbulence is of little significance compared with the difference between laminar and turbulent flow. Therefore, I conclude that the model assumption of equal viscosities was valid.

BIBLIOGRAPHY

BIBLIOGRAPHY

Carlisle, R. (1976). Personal communication. Extension Swine Specialist, University of Illinois.

Chow. (1959). Open Channel Hydraulics. McGraw-Hill, New York.

Doherty, R. L., and J. B. Franzini. (1965). Fluid Mechanics with Engineering Applications. McGraw-Hill, New York.

Einstein, H. A. (1944). ASCE Transactions, Vol. 109, p. 134.

George, R. M., and C. E. Browning. (1973). Designing gutter flushing systems for swine. ASAE Paper No. 73-4519.

Henderson. (1966). Open Channel Flow. Macmillan Co., New York.

Jones, E. E., Jr., G. B. Wilson and W. F. Schwiesow. (1971). Livestock waste management and pollution abatement. The Proceedings of the International Symposium on Livestock Wastes, Ohio State University, April 19-22, 1971. Published by ASAE.

Miller, E. C., and C. M. Hansen. (1974). Flushing. Extension Bulletin E-777, Cooperative Extension Service, Michigan State University, East Lansing, MI.

Shen, H. W. (1971). River Mechanics--Volume II. Published by author at Colorado State University, Fort Collins, CO.

Streeter, V., and E. B. Wylie. (1967). Hydraulic Transients. McGraw-Hill, New York.